Electronic structure of hole-doped delafossite oxides $CuCr_{1-x}Mg_xO_2$

T. Yokobori,[1] M. Okawa,[1] K. Konishi,[1] R. Takei,[1] K. Katayama,[1] S. Oozono,[2] T. Shinmura,[2] T. Okuda,[2] H. Wadati,[3] E. Sakai,[4] K. Ono,[4] H. Kumigashira,[4,5] M. Oshima,[6] T. Sugiyama,[7] E. Ikenaga,[7] N. Hamada,[8] and T. Saitoh[1,*]

[1]*Department of Applied Physics, Tokyo University of Science, Shinjuku, Tokyo 162-8601, Japan*
[2]*Department of Electrical and Electronics Engineering,*
Kagoshima University, Kagoshima, Kagoshima 890-0065, Japan
[3]*Department of Applied Physics and Quantum-Phase Electronics Center,*
University of Tokyo, Bunkyo, Tokyo 113-0032, Japan
[4]*Photon Factory, KEK, Tsukuba, Ibaraki 305-0801, Japan*
[5]*PRESTO, Japan Science and Technology Agency, Chiyoda, Tokyo 102-0076, Japan*
[6]*Department of Applied Chemistry, University of Tokyo, Bunkyo, Tokyo 113-8656, Japan*
[7]*Japan Synchrotron Radiation Research Institute, Sayo, Hyogo 679-5198, Japan*
[8]*Department of Physics, Tokyo University of Science, Noda, Chiba 278-8510, Japan*
(Dated: November 9, 2012)

We report the detailed electronic structure of a hole-doped delafossite oxide $CuCr_{1-x}Mg_xO_2$ ($0 \leq x \leq 0.03$) studied by photoemission spectroscopy (PES), soft x-ray absorption spectroscopy (XAS), and band structure calculations within the local-density approximation $+U$ (LDA$+U$) scheme. Cr/Cu $3p$-$3d$ resonant PES reveals that the near-Fermi level leading structure has primarily the Cr $3d$ character with a finite contribution from the Cu $3d$ through Cu $3d-$O $2p-$Cr $3d$ hybridization, having good agreement with the band structure calculations. This indicates that a doped hole will have primarily the Cr $3d$ character. Cr $2p$ PES and L-edge XAS spectra exhibit typical Cr^{3+} features for all x whereas the Cu L-edge XAS spectra exhibited a systematic change with x, now indicating that the Cu valence is monovalent at $x=0$ and the holes will be doped into the Cu sites. Nevertheless, we have surprisingly observed two types of charge-transfer satellites that should be attributed to Cu^+ ($3d^{10}$) and Cu^{2+} ($3d^9$) like initial states in Cu $2p$-$3d$ resonant PES spectrum of $CuCrO_2$, while Cu $2p$ PES spectra with no doubt shows the Cu^+ character even for the lightly doped samples. We propose that these contradictory results can be understood by introducing not only the Cu $4s$ state but also finite Cu $3d, 4s-$Cr $3d$ charge transfer via O $2p$ states in the ground-state electronic configuration.

PACS numbers: 79.60.-i, 71.20.Ps, 78.70.Dm

I. INTRODUCTION

Search for new sustainable energy resources, including new innovations, is an urgent issue in modern societies. Thermoelectricity is one of the promising candidates because there exists so much waste heat that could be recovered without sacrificing environmental costs. Delafossite-type oxides $CuMO_2$ ($M=$ trivalent cation) have considerable potential for thermoelectric materials[1] because of its layered structure of edge-shared MO_6 octahedrons that is very similar to the one in thermoelectric $NaCoO_2$.[2] Hole-doped $CuCr_{1-x}Mg_xO_2$ is a member of this family, being a candidate for a future thermoelectrode. In $CuCrO_2$, $3d^3$ electrons of the Cr^{3+} ions under the pseudo O_h local symmetry fill up the narrow Cr $3d$ $t_{2g\uparrow}$ band, which is the counterpart of the Co $3d$ t_{2g} band filled by 6 electrons in $NaCoO_2$. Hence, like in Na_xCoO_2, a rapid change in the density of states (DOS) at the Fermi level (E_F) (Ref. 3) may be realized near the t_{2g} band edge in the hole-doped system $CuCr_{1-x}Mg_xO_2$,[4] because the Cr $3d$ band is expected to be at the top of the valence band in terms of a comparison of the charge-transfer energy of the Cr^{3+} ion and that of the Cu^+ ion.[5] More precisely in k-resolved electronic structure, this situation would correspond to the pudding-mold band structure that yields a large thermopower S in Na_xCoO_2.[6] As a consequence, a combina-

tion of a large S and the highest electrical conductivity σ among delaffosite oxides[7] may be able to produce a large thermoelectric figure of merit $Z = S^2\sigma/\kappa$ (κ:thermal conductivity) in the present system.

Besides thermoelectricity, $CuMO_2$ has various interesting physical properties both in fundamental and applicational terms. A former example is multiferroic oxides $CuFeO_2$ (Ref. 8) and the present compound $CuCrO_2$ (Ref. 9) as well, whereas an important finding for the latter was a p-type transparent conducting oxide (TCO); the n-type TCO's such as In_2O_3, SnO_2 or ZnO based ones had been realized earlier,[10] yet the p-type counterpart was more difficult. A delafossite $CuAlO_2$ was the first p-type TCO with high carrier mobility and a wide band gap.[11] From the view point of the near-E_F electronic structure, this was accomplished by hole doping into a wide gap Cu^+ oxide, which has the d^{10} closed shell.[11] Hence the top of the valence band was expected to have the Cu $3d$ character with some O $2p$ one due to hybridization.

The electronic structure of $CuCrO_2$ has been investigated both theoretically and experimentally in the context of TCO,[12–14] or of thermoelectric/multiferroic materials.[15] Along the conventional strategy for TCO, the top of the valence band is expected to have mainly the Cu $3d$ character whereas it would be desirable to

have mainly the Cr $3d$ character for better thermoelectric properties as mentioned before. On this point, reported first-principles band structure calculations are still controversial; Scanlon *et al.* reported that the Cr $3d$ partial density of states (DOS) has the maximum peak at the same energy as the maximum peak of the Cu $3d$ partial DOS and negligibly small Cr $3d$ partial DOS at the top of the valence band.[12] In contrast, Maignan *et al.* reported considerable Cr $3d$ partial DOS at the top of the valence band,[15] and a recent study by Hiraga *et al.* showed the Cr $3d$ partial DOS in a much deeper energy.[14] Experimental electronic structure of CuCrO$_2$ has been investigated by photoemission spectroscopy (PES), x-ray absorption spectroscopy (XAS), and x-ray emission spectroscopy. In these studies, Scanlon *et al.* and Arnold *et al.* interpreted the development of the upper part of the valence band with x in CuAl$_{1-x}$Cr$_x$O$_2$ as a reconstruction of the Cu $3d$ bands in stead of a development of the Cr $3d$ states, and concluded that the Cr $3d$ DOS minimally contributed to the top of the valence band.[12,13] However, magnetic and transport studies reported a close coupling the doped holes by Mg substitution and the spin of the Cr ions that suggested the mixed-valences state Cr^{3+}/Cr^{4+},[1,16] which in turn implies Cr $3d$ character at the top of the valence band in the parent compound CuCrO$_2$.

From the above overview, the electronic structure of CuCr$_{1-x}$Mg$_x$O$_2$, particularly near E_F, has not been established yet. In this paper, we performed a comprehensive study on the electronic structure of lightly hole-doped CuCr$_{1-x}$Mg$_x$O$_2$ (x=0−0.03) by photoemission spectroscopy with various photon energies, soft x-ray absorption spectroscopy, and band structure calculations using the LDA+U method.

II. EXPERIMENT AND CALCULATION

Polycrystalline samples of CuCr$_{1-x}$Mg$_x$O$_2$ (x=0, 0.02, 0.03) were prepared by the standard solid-state reaction.[1] Vacuum ultraviolet (VUV)-PES measurements in the range of the Cr/Cu $3p$-$3d$ resonance ($h\nu$=40−90 eV) were performed at BL-28A of the Photon Factory, KEK, using a SCIENTA SES-2000 electron analyzer. Hard x-ray PES (HX-PES) spectra taken with $h\nu$=7940 eV were measured at BL47XU of SPring-8 using a SCIENTA R4000 electron analyzer. XAS spectra of the Cr and Cu L edge regions and Cu $2p$-$3d$ resonant soft x-ray PES (SX-PES) spectra were measured at BL-2C of the Photon Factory, KEK, using a SCIENTA SES-2000 electron analyzer. In order to obtain clean surface, we fractured the samples *in situ* right before the measurements. All the fracturings and the measurements were done in ultrahigh vacuum (better than 1.2×10^{-7} Pa) at 300K. The intensity of the resonant PES spectra was normalized using photon current of the exit mirror. The energy resolution was 30 meV (VUV-PES), 140 meV (SX-PES), and 250 meV (HX-PES). All the Fermi level (E_F) positons in the experiments were calibrated with Au spectra.

We also performed band structure calculations with the full potential linearized augmented plane-wave (FLAPW) method[17] in the local-density approximation (LDA)+U scheme.[18,19] For the effective Coulomb repulsion $U_{\text{eff}} = U - J$, relatively small values (2.0 eV for Cu and Cr) were adopted. The rhombic lattice parameters (a=2.9760 Å, c=17.1104 Å) were taken from Ref. 20. The plane-wave cut off energy was 653 eV for the wave function. We took 1313 k points in the irreducible Brillouin zone for the rhombohedral Brillouin zone.[15] Although the system is known to be antiferromagnetic,[1] the magnetic structure was assumed to be ferromagnetic[15] because the detailed magnetic structure is not experimentally well-determined.[20]

III. RESULTS

A. Experimental valence-band electronic structure compared with band structure calculations

Figure 1 shows the valence-band spectra of CuCr$_{0.98}$Mg$_{0.02}$O$_2$ taken with a series of photon energy around the Cr $3p$-$3d$ (Panel (a)) and the Cu $3p$-$3d$ (Panel (b)) resonance. One can easily observe that the intensity of the near-E_F leading structures, namely the shoulder at 1.4 eV and the peak at 2.3 eV, systematically varies with incident photon energy. This intensity evolution is displayed in Fig 1 (c) and (d) as the constant initial state (CIS) spectra at the binding energy (E_B) of 1.4 eV (Panel (c)) and 2.3 eV (Panel (d)), respectively. Panel (c) shows that the 1.4-eV shoulder exhibits a distinct resonance-type lineshape
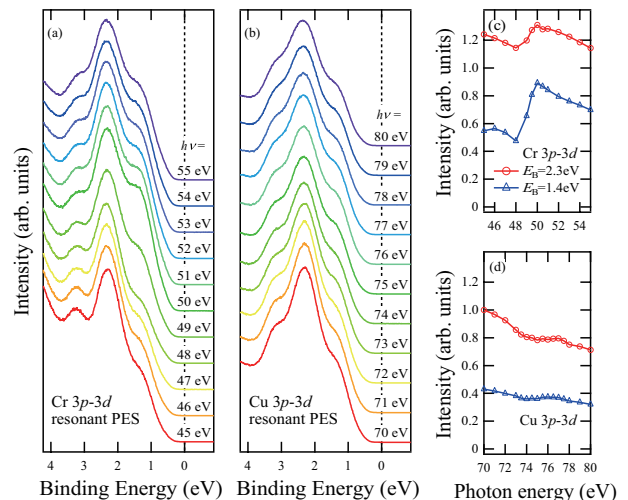

FIG. 1. Valence-band spectra of CuCr$_{0.98}$Mg$_{0.02}$O$_2$ taken with the photon energy around (a) the Cr $3p$-$3d$ resonance region and (b) the Cu $3p$-$3d$ resonance region. (c) and (d) Constant initial state spectra around the Cr $3p$-$3d$ and Cu $3p$-$3d$ resonance, respectively.

with the maximum intensity at 50.0 eV, which is the Cr $3p$-$3d$ resonance energy. In contrast, the 2.3-eV peak shows a typical weak anti resonance-type lineshape with a dip at the Cu $3p$-$3d$ resonance energy 74.0 eV, as shown in Panel (d). However, one also notices that a weak resonance of the 2.3-eV peak does exist at 50.0 eV and a tiny anti resonance of the 1.4 eV at 74.0 eV. These observations are clearly demonstrating that (1) the 1.4-eV shoulder includes a major contribution of the Cr $3d$ states with a minor contribution of the Cu $3d$ states and vice versa for the 2.3-eV peak, and (2) nevertheless there exists sizeable hybridization between the Cr $3d$ and Cu $3d$ states via O $2p$ states. The major contribution of the Cr $3d$ states in the 1.4-eV shoulder is also confirmed by a $2p$-$3d$ resonant PES measurement as shown in Fig. 2. Panel (a) demonstrates that the 1.4-eV shoulder at $h\nu$ =571 eV (off resonance) rapidly grows to an intense peak at $h\nu$ =576 eV (on resonance) with increasing photon energy. Accordingly, the on-off difference spectrum, representing the Cr $3d$ partial DOS, has a sharp peak at 1.4 eV (Panel (b)).

From the above results, the schematic energy diagram is that the Cr $3d$ is at the top of the valence band, the next is Cu $3d$, and then O $2p$ states come in the order of binding energy. This conclusion is different from recent PES[13] or optical[14] studies, both of which reported that the Cu $3d$ states are located at the top of the valence band. We note that our resonant PES experiments are more direct than theirs and hence more reliable. The present result is reasonable also from the viewpoint of the O $2p$−TM $3d$ charge transfer energy Δ because the location of the Cr $3d$ states and the Cu $3d$ states, hybridizing with each other via O $2p$ states in this compound, is governed by the difference of $\Delta_{\mathrm{Cr}^{3+}}$ and Δ_{Cu^+},[5] and $\Delta_{\mathrm{Cr}^{3+}}$

would be larger than Δ_{Cu^+} even considering the different valence and local configuration.[21,22]

In order to analyze the valence-band electronic structure in more detail, we performed LDA+U band structure calculations. Figure 3 shows the result of our LDA+U calculations. The Cu $3d$ partial DOS has intense peaks between −2.5 and −4.0 eV with small Cr $3d$ partial DOS in this range whereas the Cr $3d$ partial DOS exhibits a considerably large peak centered at about −1.5 eV, distributed from the top of the valence band to −2.5 eV with small Cu $3d$ partial DOS in this range. Here, it is noted that the calculated Cr $3d$ partial DOS has good agreement with the experimental Cr $3d$ spectral weight in Fig. 2 (b). The O $2p$ bands are mainly located below the Cr and Cu $3d$ bands, from −4 to −8 eV. All the s states, Cu $4s$, Cr $4s$ and O $2s$, show very small DOS in the entire energy range. The present calculation, par-
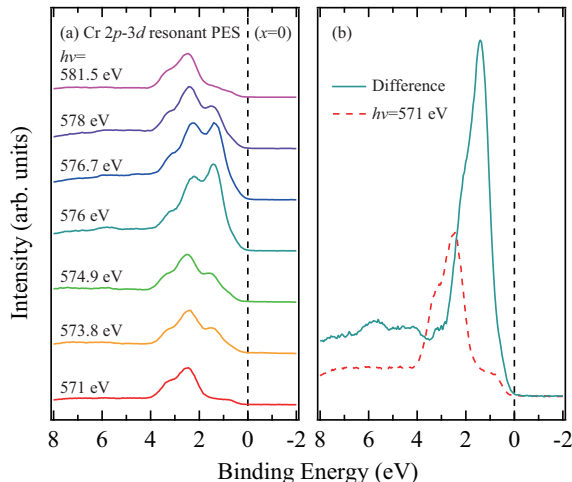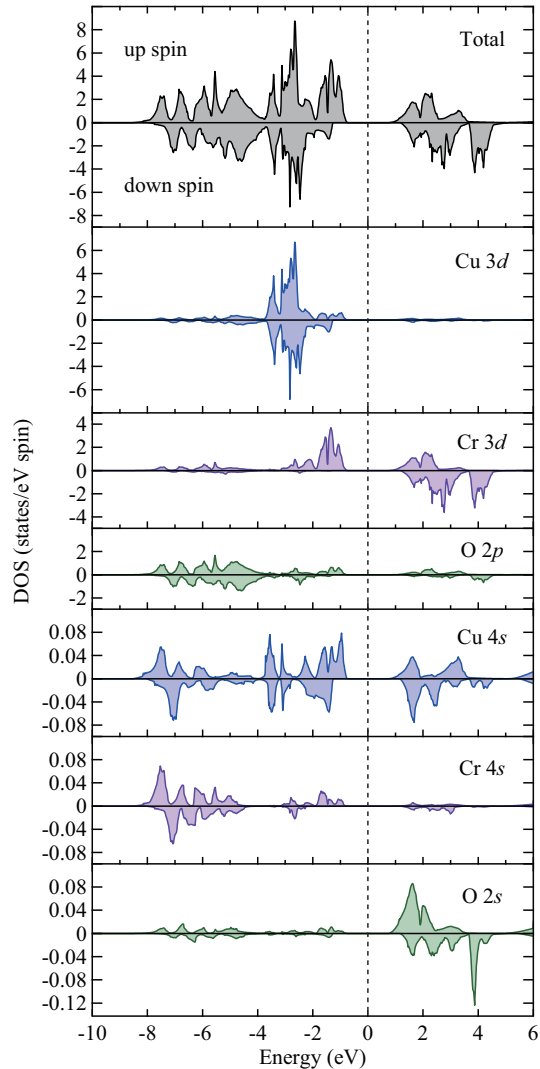

FIG. 2. (a) Valence-band spectra of CuCrO$_2$ taken with the photon energy around the Cr $2p$-$3d$ resonance region. The photon energies were determined by Cr L-edge XAS spectrum shown in Fig. 8. (b) On (576 eV)-off (571 eV) difference spectrum.

FIG. 3. LDA+U band structure calculations of CuCrO$_2$. U_{eff} was set to 2 eV both for Cr and Cu d states.

ticularly on the location of the Cu/Cr $3d$ partial DOS, completely agrees with the experimental result shown in Fig. 1 and the interpretation/prediction using the difference of $\Delta_{Cr^{3+}}$ and Δ_{Cu^+} as well.[5]

The agreement between our experiment and calculation is demonstrated more clearly in Fig. 4, which shows a comparison between the experimental spectrum of $CuCr_{0.98}Mg_{0.02}O_2$ taken at $h\nu =80$ eV and the calculated DOS.[23] The theoretical simulation curve has been constructed by broadening the cross-section-weighed total DOS with an energy dependent Lorentzian function due to the lifetime effect and a Gaussian due to the experimental resolution.[24–26] The calculated DOS shows that the leading structure at the top of the valence band (labeled as α) is dominated by the Cr $3d$ states with a minor contribution of the Cu $3d$ states whereas the most intense peak (labeled as β) primarily originates from the Cu $3d$ states. In both structures, appreciable O $2p$ DOS exist as well because of large photoionization cross section.[26] One can see that the theoretical curve satisfactorily reproduces the experimental spectrum and thus the experimental structures A to F can be assigned to the theoretical structures α to ζ, respectively.

Our calculation agrees well with the calculation by Maignan *et al.*[15] while it is different from Scanlon *et al.*[12] or Hiraga *et al.*[14] However, we note that the spectrum by Scanlon *et al.* and Arnold *et al.* can simply be interpreted by our calculation as a development of the Cr $3d$ states by Cr substitution for Al.[12,13] Hence, we consider that their experiment is actually consistent with ours. On the other hand, Hiraga *et al.* consistently interpreted
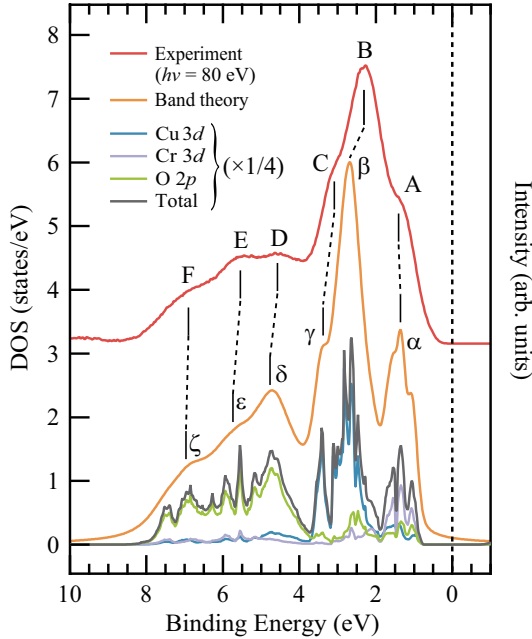
their optical absoption spectra using their band structure calculations.[14] However, optical absorption spectroscopy is indirect to probe the valence-band electronic structure because it gives the joint DOS. While we (and Maignan *et al.*) have assumed the ferromagnetic state in the calculations, we believe that the different Cr $3d$ partial DOS does not come from the different magnetic structures because both Scanlon *et al.* and Hiraga *et al.* have calculated antiferromagnetic states by the same generalized gradient approximation $+U$ (GGA$+U$) method using similar U values, yielding quite different Cr $3d$ partial DOS. Our result is also supported by another band structure calculation of $CuAl_{0.95}Cr_{0.05}O_2$ that reported the same enegetic order of the Cr and the Cu $3d$ states as ours, namely the Cr $3d$ states come to the top of the valence band by Cr doping.[27]

B. Cu and Cr valence

Figure 5 (a) shows the valence-band photoemission spectra of $CuCr_{0.98}Mg_{0.02}O_2$ taken across the resonant

FIG. 4. Comparison between the calculated DOS of $CuCrO_2$ and the valence-band spectrum of $CuCr_{0.98}Mg_{0.02}O_2$ taken at $h\nu=80.0$ eV.
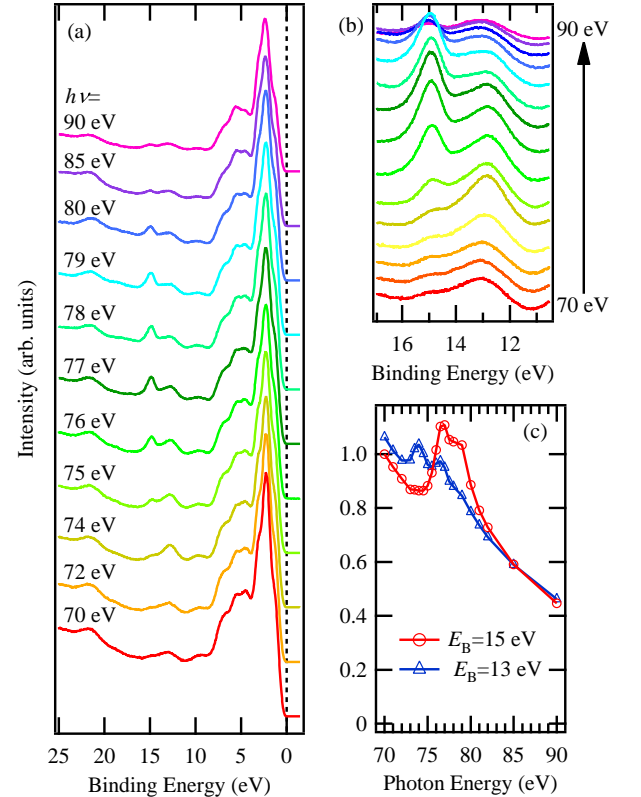

FIG. 5. (a) Wide-range valence-band spectra of $CuCr_{0.98}Mg_{0.02}O_2$ in the energy range of the Cu satellite resonances. (b) Detailed satellite structures in Panel (a). (c) CIS spectrum of the two satellite peaks at the binding energy (E_B) of 13 and 15 eV.

energies of the Cu satellite structures. There can be observed two distinct satellite peaks at the binding energy of 13 eV and 15 eV, which have their maximums at the photon energy of 74 eV and 77 eV, respectively, as shown in Panel (b). These numbers are in very good agreement with the reported satellite peaks in CuO (12.5−12.9 eV) and Cu_2O (15.3 eV), which have mainly $3d^8$ and $3d^84s$ final-state character, respectively.[28–30] The 15-eV satellite peak has also been observed in Al $K\alpha$ XPS spectra of $CuAlO_2$ and $CuCrO_2$.[13] Panel (c) shows the CIS spectra of these two satellite peaks. The CIS profiles of the satellites again well reproduce those of CuO and Cu_2O, respectively, including the two-peak structure due to $3p_{3/2}$ and $3p_{1/2}$ splitting.[28,29] All these results indicate that the doped hole in $CuCr_{0.98}Mg_{0.02}O_2$ produces Cu^{2+} ions, namely holes will be doped into the Cu sites. However, this observation seems to be incompatible with the result that the top of the valence band has mainly the Cr $3d$ character, demonstrated in Figs. 1−4. Moreover, the satellite peak at 13 eV due to Cu^{2+} seems to be too strong for only 3% doping of Mg, corresponding to 3% Cu^{2+} ions.

To confirm this observation, we performed Cu $2p$-$3d$ resonant photoemission spectroscopy measurements, as shown in Fig. 6. The excitation energies were determined by Cu L_3 XAS spectra shown in Panel (d).[31] Panel (a) shows the valence-band spectra of the $x=0$ sample taken in the Cu $2p$-$3d$ resonance region. The giant resonance peak at 15 eV is due to Cu^+ ions as seen in Fig. 5 and as reported for Cu_2O.[32] Panels (b) and (c) show the spectra taken at the photon energies before the giant resonance develops. In Panel (c), the $x=0.03$ spectrum shows the distinct 13-eV resonant peak of Fig. 5 at $h\nu=926.0$ eV that corresponds to the photon energy of the pre-peak structure in Panel (d). This hump has been observed in some Cu_2O (Ref. 33 and 34), $CuAlO_2$ (Ref. 35) and $CuCrO_2$ (Ref. 13) but has not been observed in pure Cu_2O,[36] and it is accordingly interpreted as $2\underline{p}3d^{10}$ final state due to Cu^{2+} impurity,[13,35,36] where $2\underline{p}$ denotes a core hole of the Cu $2p$ level. Therefore, both the Cu $2p$-$3d$ resonant photoemission and the Cu L_3 XAS spectra of the $x=0.03$ sample clearly demonstrate the Cu $3d$ nature of the doped holes observed in Fig. 5.

Surprisingly, however, Panel (b) shows that the $x=0$ sample, too, has the 13-eV satellite. This can never be due to Cu^{2+} impurity because the Cu L_3 XAS spectrum has no appreciable pre-peak (see Panel (d)). Here, we noted that the very slight modulation from the baseline at the pre-peak of the $x=0$ spectrum cannot explain the large 13-eV resonance peak because the Cu^{2+} impurity concentration in the $x=0.03$ sample, if exists, can be estimated to be a few percent at most by a comparison with the reported relation between the concentration and the pre-peak intensity in $CuAlO_2$.[35] Therefore, it can be undoubtedly concluded that some kind of $3d^9$ state that does not originating from Cu^{2+} impurities, should exist even in the pure $CuCrO_2$, and based on this fact, one may further go beyond the $x=0$ case, namely, the whole

portion of a doped hole may not necessary go into a Cu site even because the 13-eV satellite is observed.

Figure 7 shows Cu $2p$ core-level spectra of $CuCrO_2$ and $CuCr_{0.97}Mg_{0.03}O_2$. The $x=0$ spectrum in Panel (a) is almost identical to the reported spectra of $CuCrO_2$ (Refs. 13 and 37) and also $CuAlO_2$.[35] There is no trace of structures from the Cu^{2+} state that, if exist, can easily be identified as is the case of oxidized $CuAl_{1−x}Zn_xO_2$ or $CuRh_{1−x}Mg_xO_2$.[35,37] A reported energy shift of the Cu $2p_{3/2}$ peak due to Mg doping[13] was not observed and the $x=0.03$ spectrum is almost identical to that of $x=0$, which is very similar to what was observed in $CuAl_{1−x}Zn_xO_2$.[35] This fact raises doubt about the Cu $3d$ nature of a doped hole. Nevertheless, a small change due to Mg doping can be observed in Panel (b); the Cu $2p_{3/2}$ line shape becomes asymmetrically broad. This is reflecting an increase in metallicity of the system, particularly on the Cu sites, suggesting again the Cu $3d$ nature of a doped hole.
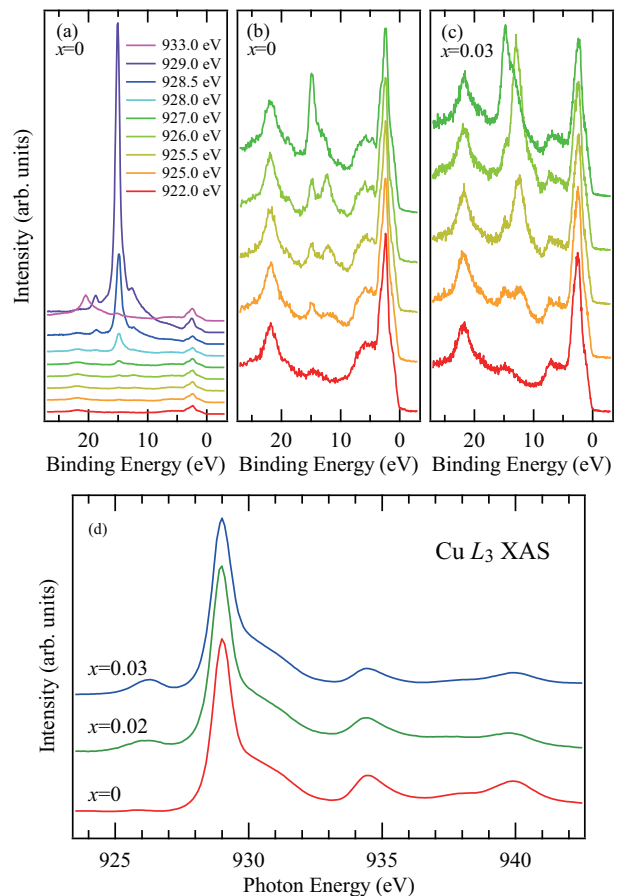

FIG. 6. Valence-band spectra of $CuCr_{1−x}Mg_xO_2$ ($x=0$, 0.03) taken with the photon energy around the Cu $2p$-$3d$ resonance region. (a) Cu $2p$-$3d$ resonant spectra of the $x=0$ sample. (b) Same as (a) around the pre-peak energy region before the giant resonance. (c) Cu $2p$-$3d$ resonant spectra of $x=0.03$ sample in the same energy region as (b). (d) Cu L_3 XAS spectra of $CuCr_{1−x}Mg_xO_2$ ($x=0$, 0.02, 0.03).
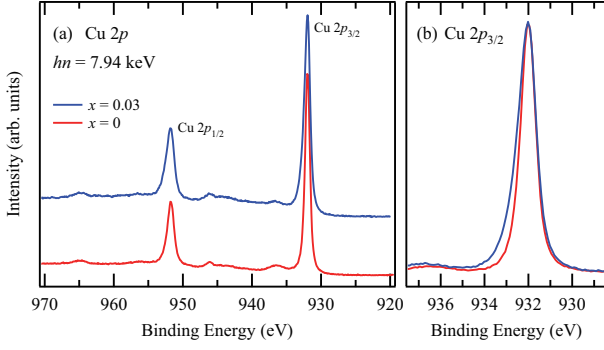
FIG. 7. (a) Cu $2p$ core-level HX-PES spectra of $CuCr_{1-x}Mg_xO_2$ ($x=0$, 0.03). (b) Comparison of the $2p_{3/2}$ peak of $x=0$ and 0.03. Note that the background due to secondary electrons were subtracted by the Shirley method.

Figure 8 shows Cr $2p$ core-level spectra of $CuCrO_2$ and $CuCr_{0.98}Mg_{0.02}O_2$. The double-peak structure observed in the Cr $2p_{3/2}$ peak of the both samples is characteristic of Cr^{3+} compound. Both the spectra in Panel (a) are indeed very similar to those of Cr_2O_3 and CrN.[38,39] The $x=0$ and 0.02 spectra are very similar to each other, displaying Cr^{3+} nature. However, the Cr $2p_{3/2}$ peak shows a remarkable change due to Mg doping; the first peak at 575 eV obviously decreases in intensity with Mg doping. A very similar change has recently been observed in CrN across its insulator-metal transition, which has been explained by the screening effects due to mobile carriers.[39] Therefore, the observed change is likely an evidence that doped holes move around the Cr sites, suggesting the Cr $3d$ nature of a doped hole. This result is consistent with the valence-band satellite analyses in Figs. 5 and 6. Nevertheless, all the three Cr $L_{2,3}$ XAS spectra in Panel (b) are very similar to the reported spectra of $LaCrO_3$ and Cr_2O_3,[40,41] indicating that the Cr ions are trivalent. Unlike the Cu L_3 edge, Cr $L_{2,3}$ XAS spectra show no detectable changes with hole doping that were observed for $La_{1-x}Sr_xCrO_3$ with $x \geq 0.3$.[40]

IV. DISSUSSION

It is already established now that the ground-state electron configuration of Cu_2O is not a simple $|3d^{10}\rangle$, but $\alpha|3d^{10}\rangle + \beta|3d^94s\rangle$, while that of CuO is described as $\alpha'|3d^9\rangle + \beta'|3d^{10}\underline{L}\rangle$, where $\underline{L}$ denotes an O $2p$ ligand hole; the d^{10} configuration of the Cu^+ ion should be spherical, but it was long ago pointed out that the charge distribution in Cu_2O can be non-spherical due to the hybridization between the $d_{3z^2-r^2}$ orbital (z axis along the Cu-O bonding) and the $4s$ orbital,[42] and has been discussed theoretically later.[43] This hybridization yields a $d_{3z^2-r^2}$ hole and hence the ground state of Cu_2O should have the $|3d^94s\rangle$ component. The d hole state has recently been directly observed,[44] confirming the interpretation of the

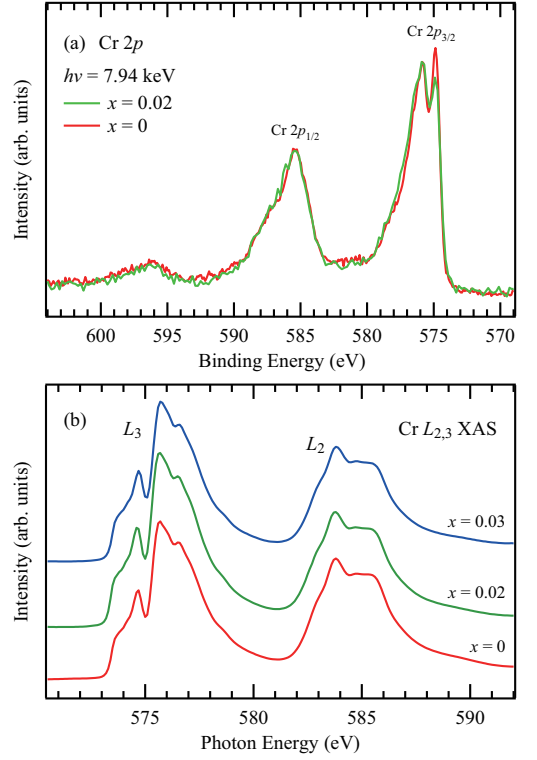FIG. 8. (a) Cr $2p$ core-level HX-PES spectra of $CuCr_{1-x}MgxO_2$ ($x=0$, 0.02). Note that the background due to secondary electrons were subtracted by the Shirley method in order to analyze the intensity change with x. (b) Cr $L_{2,3}$ XAS spectra of $CuCr_{1-x}MgxO_2$ ($x=0$, 0.02, 0.03).

satellite structures at 15 eV (the $|3d^94s\rangle \rightarrow |3d^84s\rangle$ process) in Cu_2O and at 13 eV (the $|3d^9\rangle \rightarrow |3d^8\rangle$ process) in CuO.[28–30]

The situation in $CuCrO_2$ is quite analogous to Cu_2O because the local environment around Cu is the same O-Cu-O dumb-bell structure, and therefore it is not surprizing that the ground state has the $|3d^94s\rangle$ component. What is striking in our results is that even the $x=0$ sample with no Cu^{2+} impurity centers has shown a weak but detectable 13-eV satellite (Fig. 6). This inevitablly indicates that not a "virtual" d^9 state ($|3d^94s\rangle$) but the "real" d^9 state ($|3d^9\rangle$) has to exist in $CuCrO_2$. However, the Cu $2p$ core-level spectra do not show any trace of such a configuration even for hole-doped samples, either. Nevertheless, the development of the Cu L_3 pre-peak structure with x, again, undoubtedly demonstrates that this $|3d^9\rangle$ configuration increases with x. On the other hand, the doped hole should have the Cr $3d$ character from the Cr $2p$ HX-PES spectra while the Cr L-edge XAS spectra show no detectable changes.

To understand the above contradictory results, we reconsider the local electronic structure of the Cu site beyond the nearest neighbor oxygens, namely consider the two metal sites, Cu and Cr, because their wave functions are actually connected via the O $2p$ wave functions.

Within a metal-oxygen single cluster model (CuO_2^{3-} and CrO_6^{9-} for the Cu and the Cr sites, respectively), the local electronic configuration of Cu^+ can be described as $\alpha|3d^{10}\rangle + \beta|3d^9 4s\rangle$, whereas that of Cr^{3+} will be $\alpha'|3d^3\rangle+\beta'|3d^4\underline{L}\rangle$.[22,45] Although the $\underline{L}$ molecular orbitals of the Cu and the Cr sites have in fact different symmetries, there should be sizable overlap between some of them as discussed in Fig. 1. Hence, we consider Cu-O-Cr cluster and re-define $\underline{L}$ as a O $2p$ ligand hole in a molecular orbital of this cluster. In this model, the conbination of the $|3d^9 4s\rangle$ configuration of Cu^+ and the $|3d^4\underline{L}\rangle$ configuration of Cr^{3+} can produce the $|3d^9\rangle$ and $|3d^4\rangle$ configurations at the Cu and Cr sites, respectively, becauese of the extended nature of the $4s$ state. Hence, the ground state $|g\rangle$ can be described as

$$|g\rangle = \alpha|d^{10}d^3\rangle + \beta|d^9 s\, d^3\rangle + \gamma|d^9 d^4\rangle + \delta|d^{10}\underline{L}\, d^4\rangle,$$

where the left d^9 and d^{10} denote the Cu $3d$ states, s denotes the Cu $4s$ state, and the right d^3 and d^4 denote the Cr $3d$ states. $|d^{10}d^3\rangle$ is the main configuration, $|d^9 s\, d^3\rangle$ corresponds to the $d_{3z^2-r^2}$ hole state, $|d^9 d^4\rangle$ is the Cu $4s$-to-Cr $3d$ charge transfer state, and finally $|d^{10}\underline{L}\, d^4\rangle$ originates from the O $2p$-to-Cr $3d$ charge transfer state, which is the second main configuration. The $|d^9 s\,\underline{L}\, d^4\rangle$ configuration is not included because this is the origin of the $|d^9 d^4\rangle$ configuration.

The final state of the valence-band photoemission by Cu $3d$ emission is

$$|f_{\mathrm{v}}^{\mathrm{Cu}}\rangle = a|d^{10}\underline{L}\, d^3\rangle + b|d^9 d^3\rangle + c|d^8 s\, d^3\rangle + d|d^8 d^4\rangle.$$

Here, $|d^9\underline{L}\, d^4\rangle$ is neglected because this configuration will easily transform into $|d^9 d^3\rangle$ due to the combination of one extra electron at the Cr site and the lack of one electron at the Cu site.

For the Cu $2p$ core-level photoemission, the final state will be

$$|f_{\mathrm{c}}^{\mathrm{Cu}}\rangle = a|\underline{c}d^{10}d^3\rangle + b|\underline{c}d^9 s\, d^3\rangle + c|\underline{c}d^{10}\underline{L}\, d^4\rangle + d|\underline{c}d^9 d^4\rangle,$$

and for the Cu L-edge XAS, the final state will be

$$|f_{L}^{\mathrm{Cu}}\rangle = a|\underline{c}d^{10}s\, d^3\rangle + b|\underline{c}d^{10}d^4\rangle + c|\underline{c}d^{10}s\,\underline{L}\, d^4\rangle,$$

where $\underline{c}$ denotes a Cu $2p$ core hole.

Within this framework, the Cu $3p$-$3d$ and $2p$-$3d$ resonant photoemission spectra can have both the $3d^8 4s$ (at 15 eV) and $3d^8$ (at 13 eV) final state satellites due to the processes of $|d^9 s\, d^3\rangle \rightarrow |d^8 s\, d^3\rangle$ and $|d^9 d^4\rangle \rightarrow |d^8 d^4\rangle$, respectively. This scenario even predicts that $CuAlO_2$ will not have the 13 eV satellite because there are no available Al states in the valence band, and indeed, an XPS spectrum of $CuAlO_2$ shows a dip around 13 eV while that of $CuCrO_2$ has extra spectral weight,[13] supporting the scenario. The absence of the $|\underline{c}3d^9\rangle$ final state satellite in the Cu $2p$ core-level spectra can be explained by strong screening effects due to the presence of a core hole at the Cu site: The large $\underline{c}$-d Coulomb attraction increases the number of d electrons and accordingly it makes the
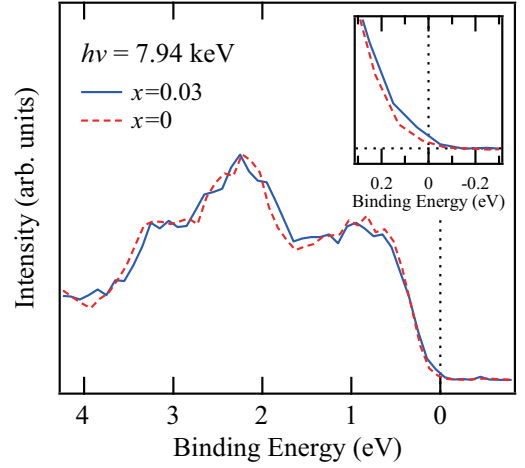

FIG. 9. Near-E_F valence-band spectra of $CuCr_{1-x}Mg_xO_2$ ($x=0$, 0.03) taken with 7.94 keV. The intensity is normalized with respect to the spectral weight sum from -0.5 to 4.0 eV.

$|\underline{c}d^9 s\, d^3\rangle$ and $|\underline{c}d^9 d^4\rangle$ weight negligible even for the lightly hole-doped samples. Likewise, the lack of the pre-peak structure in the Cu L-edge XAS specturm of the $x=0$ sample can also be explained by the core-hole screening effects that reduce the weight of the $|\underline{c}d^{10}d^4\rangle$ (and the $|\underline{c}d^{10}s\,\underline{L}\, d^4\rangle$) configuration(s) in $|f_L^{\mathrm{Cu}}\rangle$ (Fig. 6 (b)).

From the above consideration, there must be weak but finite Cu $4s$ spectral weight at the top of the valence band, and this can actually be observed; Figure 9 shows a HX-PES valence-band spectra of $x=0$ and 0.03 samples. Considering that the photoionization cross section of sp states of this energy range is largely enhanced,[26] the small enhancement at very near E_F (see the inset) can be interpreted as an increase in the Cu $4sp$ emission due to hole doping, namely, supporting finite Cu $4s$ spectral weight at the top of the valence band. It is accordingly revealed that the very top of the valence band has actually the Cu $4s$ character in addition to the Cr $3d$ character. This Cu $4s$−Cr $3d$ duality of a doped hole can explain the observed magnetic and transport properties of $CuCr_{1-x}Mg_xO_2$; the doped holes moving in the Cr-O network can lift the magnetic frustration in the Cr triangular spin lattice, resulting in an increase in the magnetic susceptibility with x.[1] The holes that are not restricted in the Cu-O network also explain a higher electric conductivity compared with other hole-doped Cu delafossites like $CuAlO_2$.[7] In particular, the highest conductivity by selecting Cr^{3+} is strikingly demonstrating that the importance of the Cu-Cr combination.[7] From the viewpoint of the electronic structure, this can be interpreted as a consequence of an "appropriate" combination in terms of the difference of $\Delta_{M^{3+}}$ and Δ_{Cu^+} of $CuMO_2$.[5]

V. CONCLUSIONS

We have studied the electronic structure of hole-doped delafossite oxides $CuCr_{1-x}Mg_xO_2$ by high-resolution photoemission spectroscopy, x-ray absorption spectroscopy, and LDA+U band-structure calculations. The Cr and Cu 3p-3d resonant PES spectra demonstrated that the leading structure of the valence band near the E_F has primarily the Cr 3d character with a minor contribution from the Cu 3d due to hybridization with the O 2p states, having good agreement with the band structure calculation. This result indicates that a doped hole will primarily have the Cr 3d character. The Cr 2p PES and L-edge XAS spectra of $CuCr_{1-x}Mg_xO_2$ always showed typical Cr^{3+} features whereas the Cu L-edge XAS spectra exhibited a systematic change with x. This result, by contrast, indicates that the Cu valence is monovalent at $x=0$ and the holes will be doped into the Cu sites, which contradicts the Cr and Cu 3p-3d resonant PES. Nevertheless, the Cu 2p-3d resonant PES spectra display the two types of charge-transfer satellites that should be attributed to Cu^+ ($3d^{10}$) and Cu^{2+} ($3d^9$) like initial states, while the Cu 2p PES with no doubt shows the Cu^+ character even for $x > 0$.

We have proposed that the above apparently contradictory results can consistently be understood by introducing not only the Cu 4s state as traditionally, but also newly finite Cu 4s−Cr 3d charge transfer via O 2p states in the ground-state electronic configuration, which can further explain well some of the important magnetic and transport properties.

* Author to whom correspondence should be addressed. Electronic address: t-saitoh@rs.kagu.tus.ac.jp

[1] T. Okuda, N. Jufuku, S. Hidaka, and N. Terada, Phys. Rev. B **72**, 144403 (2005).

[2] I. Terasaki, Y. Sasago, and K. Uchinokura, Phys. Rev. B **56**, R12685 (1997).

[3] T. Takeuchi, T. Kondo, T. Takami, H. Takahashi, H. Ikuta, U. Mizutani, K. Soda, R. Funahashi, M. Shikano, M. Mikami, S. Tsuda, T. Yokoya, S. Shin, and T. Muro, Phys. Rev. B **69**, 125410 (2004).

[4] The doped hole amount is $x/(1 - x)$.

[5] H. Iwasawa, K. Yamakawa, T. Saitoh, J. Inaba, T. Katsufuji, M. Higashiguchi, K. Shimada, H. Namatame, and M. Taniguchi, Phys. Rev. Lett. **96**, 067203 (2006).

[6] K. Kuroki and R. Arita, J. Phys. Soc. Jpn. **76**, 083707 (2007).

[7] R. Nagarajan, A. Draeseke, A. Sleight, and J. Tate, J. Appl. Phys. **89**, 8022 (2001).

[8] T. Kimura, J. C. Lashley, and A. P. Ramirez, Phys. Rev. B **73**, 220401(R) (2006).

[9] S. Seki, Y. Onose, and Y. Tokura, Phys. Rev. Lett. **101**, 067204 (2008).

[10] I. Hamberg and C. G. Granqvist, J. Appl. Phys. **60**, R123 (1986).

[11] H. Kawazoe, M. Yasukawa, H. Hyodo, M. Kurita, H. Yanagi, and H. Hosono, Nature **389**, 939 (1997).

[12] D. O. Scanlon, A. Walsh, B. J. Morgan, G. W. Watson, D. J. Payne, and R. G. Egdell, Phys. Rev. B **79**, 035101 (2009).

[13] T. Arnold, D. J. Payne, A. Bourlange, J. P. Hu, R. G. Egdell, L. F. J. Piper, L. Colakerol, A. De Masi, P.-A. Glans, T. Learmonth, K. E. Smith, J. Guo, D. O. Scanlon, A. Walsh, B. J. Morgan, and G. W. Watson, Phys. Rev. B **79**, 075102 (2009).

[14] H. Hiraga, T. Makino, T. Fukumura, H. Weng, and M. Kawasaki, Phys. Rev. B **84**, 041411(R) (2011).

[15] A. Maignan, C. Martin, R. Frésard, V. Eyert, E. Guilmeau, S. Hébert, M. Poienar, and D. Pelloquin, Solid State Commun. **149**, 962 (2009).

[16] Y. Ono, K. Satoh, T. Nozaki, and T. Kajitani, Jpn. J. Appl. Phys. **46**, 1071 (2007).

[17] O. K. Andersen, Phys. Rev. B **12**, 3060 (1975); T. Takeda and J. Kubler, J. Phys. F: Met. Phys. **9**, 661 (1979).

[18] P. Hohenberg and W. W. Kohn, Phys. Rev. **136**, B864 (1964); W. Kohn and L. J. Sham, *ibid*. **140**, A1133 (1965); S. H. Vosko, L. Wilk, and M. Nusair, Can. J. Phys. **58**, 1200 (1980).

[19] V. I. Anisimov, J. Zaanen, and O. K. Andersen, Phys. Rev. B **44**, 943 (1991); I. Solovyev, N. Hamada, and K. Terakura, *ibid*. **53**, 7158 (1996); V. I. Anisimov, F. Aryasetiawan, and A. I. Linchtenstein, J. Phys.: Condens. Matter **9**, 767 (1997).

[20] M. Poienar, F. Damay, C. Martin, V. Hardy, A. Maignan, and G. André, Phys. Rev. B **79**, 014412 (2009).

[21] A. Fujimori, A. E. Bocquet, T. Saitoh, and T. Mizokawa, J. Electron Spectrosc. Relat. Phenomen. **62**, 141 (1993).

[22] T. Saitoh, A. E. Bocquet, T. Mizokawa, and A. Fujimori, Phys. Rev. B **52**, 7934 (1995).

[23] A $x=0.02$ spectrum is compared with theory because of a lower quality of $x=0.00$ spectra in this photon energy range.

[24] T. Saitoh, T. Mizokawa, A. Fujimori, M. Abbate, Y. Takeda, and M. Takano, Phys. Rev. B **55**, 4257 (1997).

[25] H. Iwasawa, S. Kaneyoshi, K. Kurahashi, T. Saitoh, I. Hase, T. Katsufuji, K. Shimada, H. Namatame, and M. Taniguchi, Phys. Rev. B **80**, 125122 (2009).

[26] J. J. Yeh and I. Lindau, At. Data Nucl. Data Tables **32**, 1 (1985).

[27] H. Kizaki, K. Sato, A. Yanase, and H. Katayama-Yoshida, Jpn. J. Appl. Phys. **44**, L1187 (2005).

[28] M. R. Thuler, R. L. Benbow, and Z. Hurych, Phys. Rev. B **26**, 669 (1982).

[29] J. Ghijsen, L. H. Tjeng, H. Eskes, G. A. Sawatzky, and R. L. Johnson, Phys. Rev. B **42**, 2268 (1990).

[30] Z.-X. Shen, R. S. List, D. S. Dessau, F. Parmigiani, A. J. Arko, R. Bartlett, B. O. Wells, I. Lindau, and W. E. Spicer, Phys. Rev. B **42**, 8081 (1990).

[31] Because of a problem of energy calibration, our photon energy of the Cu L_3 XAS spectra is a little different from the reported values for $CuCrO_2$ or Cu_2O (Refs. 13, 32, 34, and 36).

[32] L. H. Tjeng, C. T. Chen, and S.-W. Cheong, Phys. Rev. B **45**, 8205 (1992).

[33] S. L. Hulbert, B. A. Bunker, F. C. Brown, and P. Pianetta, Phys. Rev. B **30**, 2120 (1984).

[34] M. Grioni, J. B. Goedkoop, R. Schoorl, F. M. F. de Groot, J. C. Fuggle, F. Schäfers, E. E. Koch, G. Rossi, J.-M. Esteva, and R. C. Karnatak, Phys. Rev. B **39**, 1541 (1989).

[35] D. J. Aston, D. J. Payne, A. J. H. Green, R. G. Egdell, D. S. L. Law, J. Guo, P. A. Glans, T. Learmonth, and K. E. Smith, Phys. Rev. B **72**, 195115 (2005).

[36] M. Grioni, J. F. van Acker, M. T. Czyzyk, and J. C. Fuggle, Phys. Rev. B **45**, 3309 (1992).

[37] T. K. Le, D. Flahaut, H. Martinez, N. Andreu, D. Gonbeau, E. Pachoud, D. Pelloquin, and A. Maignan, J. Solid State Chem. **184**, 2387 (2011).

[38] M. C. Biesinger, C. Brown, J. R. Mycroft, R. D. Davidson, and N. S. McIntyre, Surf. Interface Anal. **36**, 1550 (2004).

[39] P. A. Bhobe, A. Chainani, M. Taguchi, T. Takeuchi, R. Eguchi, M. Matsunami, K. Ishizaka, Y. Takata, M. Oura, Y. Senba, H. Ohashi, Y. Nishino, M. Yabashi, K. Tamasaku, T. Ishikawa, K. Takenaka, H. Takagi, and S. Shin, Phys. Rev. Lett. **104**, 236404 (2010).

[40] D. D. Sarma, K. Maiti, E. Vescovo, C. Carbone, W. Eberhardt, O. Rader, and W. Gudat, Phys. Rev. B **53**, 13369 (1996).

[41] M. Matsubara, T. Uozumi, A. Kotani, Y. Harada, and S. Shin, J. Phys. Soc. Jpn. **71**, 347 (2002).

[42] L. E. Orgel, J. Chem. Soc., 4186 (1958).

[43] P. Marksteiner, P. Blaha, and K. Schwarz, Z. Phys. B **64**, 119 (1986).

[44] J. M. Zuo, M. Kim, M. O'Keeffe, and J. C. H. Spence, Nature **401**, 49 (1999).

[45] T. Uozumi, K. Okada, A. Kotani, R. Zimmermann, P. Steiner, S. Hüfner, Y. Tezuka, and S. Shin, J. Elecctron Spectrsc. Relat. Phenom. **83**, 9 (1997).